Translational Oncology

www.transonc.com

Volume 5 Number 2 April 2012 pp. 77–84 77

Development of a Novel Preclinical Pancreatic Cancer Research Model: Bioluminescence Image–Guided Focal Irradiation and Tumor Monitoring of Orthotopic Xenografts[1]

Richard Tuli*,[2], Andrew Surmak*, Juvenal Reyes*, Amy Hacker-Prietz*, Michael Armour*, Ashley Leubner†, Amanda Blackford†, Erik Tryggestad*, Elizabeth M. Jaffee†, John Wong*, Theodore L. DeWeese*,† and Joseph M. Herman*

*Department of Radiation Oncology & Molecular Radiation Sciences, Johns Hopkins University School of Medicine, Baltimore, MD, USA; †Department of Oncology, Johns Hopkins University School of Medicine, Baltimore, MD, USA

Abstract

PURPOSE: We report on a novel preclinical pancreatic cancer research model that uses bioluminescence imaging (BLI)–guided irradiation of orthotopic xenograft tumors, sparing of surrounding normal tissues, and quantitative, noninvasive longitudinal assessment of treatment response. *MATERIALS AND METHODS:* Luciferase-expressing MiaPaCa-2 pancreatic carcinoma cells were orthotopically injected in nude mice. BLI was compared to pathologic tumor volume, and photon emission was assessed over time. BLI was correlated to positron emission tomography (PET)/computed tomography (CT) to estimate tumor dimensions. BLI and cone-beam CT (CBCT) were used to compare tumor centroid location and estimate setup error. BLI and CBCT fusion was performed to guide irradiation of tumors using the small animal radiation research platform (SARRP). DNA damage was assessed by γ-H2Ax staining. BLI was used to longitudinally monitor treatment response. *RESULTS:* Bioluminescence predicted tumor volume ($R = 0.8984$) and increased linearly as a function of time up to a 10-fold increase in tumor burden. BLI correlated with PET/CT and necropsy specimen in size ($P < .05$). Two-dimensional BLI centroid accuracy was 3.5 mm relative to CBCT. BLI-guided irradiated pancreatic tumors stained positively for γ-H2Ax, whereas surrounding normal tissues were spared. Longitudinal assessment of irradiated tumors with BLI revealed significant tumor growth delay of 20 days relative to controls. *CONCLUSIONS:* We have successfully applied the SARRP to a bioluminescent, orthotopic preclinical pancreas cancer model to noninvasively: 1) allow the identification of tumor burden before therapy, 2) facilitate image-guided focal radiation therapy, and 3) allow normalization of tumor burden and longitudinal assessment of treatment response.

Translational Oncology (2012) 5, 77–84

Introduction

Pancreatic cancer is the fourth leading cause of cancer-related deaths in the United States with an overall relative survival rate of 5% at 5 years [1]. Although most clinical trials have substantiated the modest clinical benefit of gemcitabine-based chemotherapy, the role of radiation in the adjuvant and definitive setting remains controversial [2,3]. Unfortunately, most randomized trials studying the addition of molecular targeting agents, gene therapy, and immunotherapy have also failed to show meaningful benefit [4]. As a result, clinical trials with a higher likelihood for success need to be designed using more effective multimodal treatment strategies. Whereas preclinical animal

Address all correspondence to: Joseph M. Herman, MD, MSc, Department of Radiation Oncology & Molecular Radiation Sciences, 401 N Broadway, Suite 1440, Baltimore, MD 21231-6681. E-mail: jherma15@jhmi.edu

[1]The authors thank ProQinase GmbH for providing the Mia PaCa-2–ELN cell line, as well as The Claudio X. Gonzalez Family Foundation and many patients and families whose generous donations made this research possible. J.W. has a research funding and consultation agreements with Xstrahl, Inc.

[2]Dr Tuli is now affiliated with the Department of Radiation Oncology, Cedars-Sinai Medical Center, Los Angeles, CA.

Received 26 October 2011; Revised 7 December 2011; Accepted 7 December 2011

1944-7124/12 DOI 10.1593/tlo.11316

research is integral to the development of such therapies, available models are far from optimal. Technological advances made in human conformal radiation treatment have significantly outpaced those for laboratory animal research, which is often nonlocalized, single-beam irradiation of large fields due to lack of accurate targeting and delivery. Recognizing the pressing need to bridge this translational gap for radiation research, several groups have initiated development of small animal irradiators [5,6]. Our group has developed a small animal radiation research platform (SARRP) incorporating: 1) a gantry and robotic stage that supports isocentric and noncoplanar conformal irradiation and 2) on-board cone-beam CT (CBCT) guidance to facilitate coregistration with other imaging and accurate repositioning for fractionated therapy [7]. While suitable for superficial targets and those with adequate radiographic contrast, such as in the lung or where bony landmarks can be used as a surrogate, CBCT is not optimal to precisely localize orthotopic, intrathoracic, and intra-abdominal tumors owing to the lack of soft tissue contrast and functional tumor imaging. Similar to clinical applications, a complementary soft tissue imaging modality could help facilitate precise delineation of the tumor and its margins. BLI has emerged as a noninvasive means of longitudinal *in vivo* assessment of tumors, as well as response to therapy in preclinical models [8]. Although BLI has become an integral component of preclinical tumor models, its application to date with radiation has been limited [9]. Biologically relevant tumor models are also an essential component of preclinical studies. Subcutaneous xenograft models are the most commonly used modality for preclinical experimental therapeutics because they represent a convenient platform for monitoring tumor growth and response to therapy. However, they are less than ideal for translational research on pancreatic tumors secondary to their inability to faithfully recapitulate the tumor microenvironment and locally invasive and metastatic nature of the disease [10].

Herein, we report on a novel approach to preclinical pancreatic cancer radiation research that allows BLI-guided irradiation of orthotopic xenograft tumors, sparing of surrounding normal tissues and quantitative, noninvasive assessment of treatment response. This unique translational model is currently being used to successfully investigate the mechanisms of action and efficacy of chemotherapeutic and targeted agents with focused radiation for pancreatic cancer.

Materials and Methods

Animal Xenografts

Female athymic nude mice (4 weeks old; Harlan Sprague-Dawley, Madison, WI) were used in accordance with institutional guidelines under approved protocols. The MiaPaCa-2 pancreas carcinoma cell line stably transfected with the luciferase-aminoglycoside phosphotransferase fusion gene under the control of the elongation factor (EF)-1α promoter (MiaPaCa-2–ELN) was kindly provided by Dr Ralph Graeser, ProQinase GMBH, Freiburg, Germany [11]. Mice were anesthetized by intraperitoneal injection of 75 mg/kg ketamine and 7.5 mg/kg xylazine before surgery and treatment. Subcutaneous flank tumors were generated bilaterally by injection of 1×10^6 MiaPaCa-2–ELN cells in 100 μl of phosphate-buffered saline per flank. Tumor dimensions and animal weights were measured twice per week. Tumor volume was calculated according to the equation for a prolate spheroid ($(\pi/6) \times (L \times W^2)$), where L and W are the longer and shorter dimensions of the tumor, respectively. Tumor growth inhibition (TGI) and tumor growth delay were determined by reduction in volume, as previously described [12]. Orthotopic pancreatic tumors were generated by injection of 1 to 2×10^6 MiaPaCa-2–ELN cells into the tail of the pancreas. Mice were killed when moribund, if they experienced a change in body weight of 20% of pretreatment weight, or if tumor size/burden exceeded 10 times the pretreatment volume.

Tumor Imaging

Small animal positron emission tomographic/computed tomographic (PET/CT; Philips Mosaic HP, Sunnyvale, CA) images of overnight-fasted, anesthetized mice with orthotopic tumors were obtained after intravenous (IV) injection of 10 MBq of ^{18}F-fluorodeoxyglucose with an uptake time of 60 minutes and static acquisition of 15 minutes. Corresponding small animal CT images were acquired, fused, and registered with PET images per standard protocol. Tumor regions of interest (ROIs) were identified after calculating standardized uptake values normalized to the liver, and tumor dimensions (length and width) were recorded.

For BLI, anesthetized mice bearing subcutaneous flank or orthotopic tumors were injected intraperitoneally with 150 mg/kg of D-luciferin (Gold Biotechnology, St Louis, MO) and optically imaged after 10 minutes using the IVIS 100 (Xenogen Corp, Alameda, CA). The pseudocolor image representing the spatial distribution of detected photons was overlaid on a grayscale photographic image. An ROI was created around the optical tumor image so that the luminescence at the edge of the circle was 5% of the peak intensity of that region. Signal intensity was quantified within an identified ROI in photons/second/squared centimeter/steradian (p/s/cm^2/Sr) after a 10-second exposure using Living Image software (Xenogen Corp).

Statistical Analysis

Maximum cross-sectional length and width in the coronal plane of PET-CT and BLI images (n = 8) were measured, used to calculate area and volume, and correlated to pathologic tumor specimen at necropsy, as described above, using Pearson correlation coefficient. Nonlinear regression plots were used to describe the correlation between bioluminescent photon emission and caliper volume measurements of tumors.

Luminescent Source Localization

A 5-mm-diameter glass bulb was filled with 5×10^5 MiaPaCa-2–ELN cells, injected with D-luciferin and sutured to the tail of the pancreas of an euthanized mouse (n = 6). The abdomen was sutured closed, and the centroid of the bulb was identified in the following ways: 1) an opaque fiducial placed on the skin surface of the mouse to visually approximate its location or 2) two-dimensional (2D) surface BLI. CBCT images of the mice were acquired on the SARRP to localize the actual centroid of the bulb and coregistered with the two methods described above. The radial distance between centroids was then measured and compared.

Tumor Irradiation

Five days after tumor implantation, mice were imaged with 2D bioluminescence and transported to the SARRP where CBCT images of anesthetized mice were acquired. Using the guidance software utility of the SARRP, BLI and CBCT images were coregistered by manual fusion; the isocenter of the tumor was identified and aligned with the central axis of the beam. Mice were irradiated with the SARRP using 225 kV (peak) x-ray beams at a dose rate of 2.5 Gy/min using

collimator of various diameters with a single anterior-posterior beam under the guidance of CBCT. Mice bearing flank tumors were randomized to receive one of the following treatments: 1) no radiation – control; 2) 5 Gy × 1 fraction; 3) 5 Gy × 2 fractions, 1 fraction daily; and 4) 5 Gy × 3 fractions, 1 fraction daily. The dose that resulted in an intermediate level of tumor growth delay was identified and selected for subsequent irradiation of orthotopic tumors.

Histologic and Immunofluorescent Staining

One hour after BLI-guided irradiation of orthotopic tumors, whole-body perfusion fixation of anesthetized mice was performed using 4% paraformaldehyde injection into the left ventricle per established protocol [13]. Once perfusion was complete, the abdominal contents were processed 1 of 2 ways. The entire abdomen with skin intact was separated from the thorax and pelvis, so as to keep organs in their native position, incubated in 30% sucrose for 24 hours, embedded in optimum cutting temperature, and sectioned using a cryostat microtome at –20°C. Alternatively, after perfusion fixation, the tumor specimen and surrounding abdominal organs were individually dissected, placed in 4% paraformaldehyde for 24 hours, paraffin embedded, and sectioned.

Immunofluorescent detection of γ-H2Ax was performed after permeabilization with 0.05% Triton in Tween-20 (Roche, Mannheim, Germany) for 1 minute after deparaffinization with xylene and rehydration with ethanol. Slides were steamed for 45 minutes at 95°C for antigen retrieval, placed in 3% bovine serum albumin overnight, incubated with mouse anti–phospho-histone H2Ax (Ser139; Cell Signaling Technology, Danvers, MA), and followed by goat antimouse Alexa Fluor 594 secondary antibody (Molecular Probes, Eugene, OR). Nuclei were counterstained with 4′,6-diamidino-2-phenylindole dihydrochloride solution (Invitrogen, Carlsbad, CA), and coverslips were mounted with Vectashield (Vector Laboratories, Peterborough, United Kingdom). The edges of coverslips were sealed with clear nail polish. Imaging was performed in the dark with confocal microscopy equipped with filter blocks for excitation of red, green, and blue fluorescence. Individual nuclei and γ-H2Ax-foci were counted by a single operator to minimize variability. Six separate regions within each analyzed specimen of irradiated and unirradiated tissue containing a minimum of 40 cells were identified, and data were reported as the average sum of foci divided by average number of nuclei.

Results

Correlation of Bioluminescence with PET/CT and Tumor Volume

As an initial experiment, subcutaneous bioluminescent xenografts were used to assess the limits of detection and relationship to physical volume of tumors. Injection of MiaPaCa-2–ELN cells into the bilateral flanks of athymic mice resulted in 100% engraftment and growth of tumors, which were subsequently imaged for bioluminescence and measured with calipers biweekly. There was significant linear correlation (R = 0.8984) between bioluminescent photon counts and measured tumor volume as noted by linear regression analysis (Figure 1*A*). In addition, mean photon counts measured as a function of time were normalized to baseline values obtained 3 days after tumor implantation (noted as day 0). Photon counts increased linearly as a function of time until approximately day 20 when values began to plateau after an approximate 10-fold increase in normalized luminescence (Figure 1*B*). As a result, a 10× increase in relative tumor burden, as measured by BLI, was used as an end point for subsequent experiments.

In an attempt to validate BLI as a molecular imaging surrogate for viable tumor detection and assessment of physical tumor size, we correlated tumor BLI to PET/CT and pathologic measurements at necropsy. Orthotopically injected MiaPaCa-2–ELN tumors were engrafted into the pancreatic tail in 100% of specimens without any associated morbidity or mortality. Tumors were detectable by both BLI and PET/CT a minimum of 3 days after implantation and were formally assessed at days 5 and 10 by all three modalities. Using Pearson coefficient, greatest length, width, and cross-sectional area of the 95% bioluminescent image was correlated to that of PET/CT and pathologic specimen (Table 1). There was excellent length and width correlation between BLI and PET/CT (R = 0.94 and R = 0.96, respectively). Whereas both BLI and PET/CT tumor lengths correlated moderately well with necropsy specimen (R = 0.80 and R = 0.87, respectively), they did not correlate well with regard to tumor widths (R = 0.64 and R = 0.68, respectively). Comparison of cross-sectional area also showed good correlation among all three modalities (Table 1). Bioluminescence and PET/CT were equally sensitive in detecting the presence of metastatic lesions from primary orthotopic tumors as confirmed pathologically at time of necropsy. Most metastases were identified macroscopically in the liver, spleen, and lung.

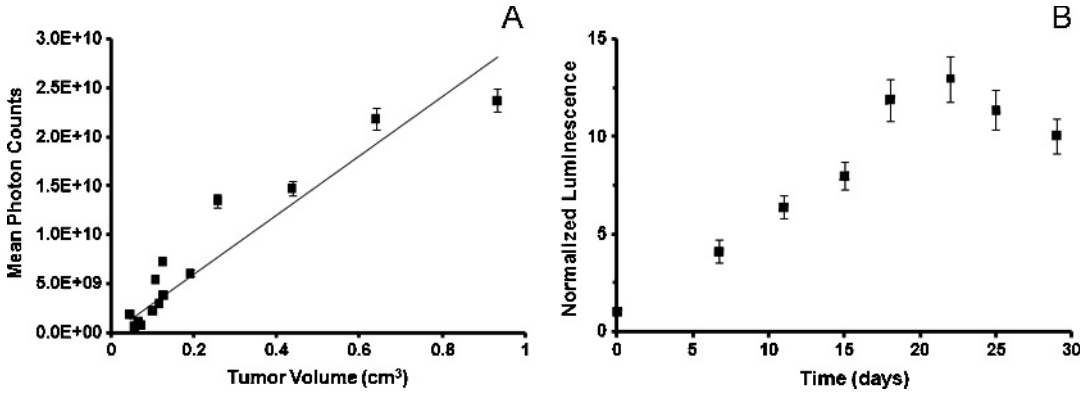

Figure 1. BLI accurately predicts tumor volume (A). Mean photon counts (p/s/cm^2/Sr) of MiaPaCa-2–ELN heterotopic tumors of varying sizes correlated well with measured tumor volume as noted by linear regression analysis (R = 0.8984; A). Normalized luminescence of pancreatic tumors was determined as a function of time and shows a relatively linear increase in signal up to 10-fold after which plateaued growth was noted (B).

Table 1. Pearson Correlation Coefficient of Orthotopic Tumor Measurements.

Measurement Method	Measurement Type	Correlation	95% CI	*P*
BLI *vs* PET/CT	Length	0.94	0.65-0.99	.002*
BLI *vs* necropsy	Length	0.80	0.11-0.97	.032*
PET *vs* necropsy	Length	0.87	0.33-0.98	.011*
BLI *vs* PET/CT	Width	0.96	0.73-0.99	.001*
BLI *vs* necropsy	Width	0.64	0.22-0.94	.122
PET *vs* necropsy	Width	0.68	0.14-0.95	.090
BLI *vs* PET/CT	Area	0.97	0.78-10.0	.001*
BLI *vs* necropsy	Area	0.79	0.09-0.97	.035*
PET *vs* necropsy	Area	0.83	0.19-0.97	.022*

CI indicates confidence interval.
*$P < .05$.

Luminescent Source Localization

We then attempted to determine whether the visually perceived centroid of the bioluminescent image was representative of the physical tumor centroid identified on CBCT using an orthotopically placed, fixed-size source of luminescence. These data would facilitate accurate placement of the radiation beam isocenter and aid in determining the potential animal positioning and setup error associated with fusion of the two imaging modalities (n = 4/group). A significant deviation of 5.8 mm was noted between the skin surface marker and the center of the bulb as identified on CBCT. This deviation margin decreased to 3.5 mm when 2D offline BLI was fused to the CBCT image. As a result, 2D bioluminescent images were used for tumor localization and image guidance with a radial margin of 4 mm applied to the tumor volume to create a pseudo-"planning target volume" (PTV; Figure 2). To cover this volume, average collimator sizes used ranged from 10 to 15 mm in diameter when a 4-mm radial margin was applied to the gross tumor volume as determined from the 95% bioluminescent image fused to the CBCT image.

Determining Tumor Response to Irradiation

Using a 10-fold increase in normalized luminescence as an end point (as previously determined), subcutaneous flank tumors were left untreated or treated with varying radiation doses to identify the dose that would result in an intermediate, yet significant, level of TGI without significant toxicity (Figure 3). Irradiation with 5 Gy, 5 Gy × 2 fractions, and 5 Gy × 3 fractions led to growth delays of 31, 57.5, and 60 days, respectively, relative to untreated controls (n = 4/group, $P < .05$). Whereas growth delays seen with cumulative doses of 10 and 15 Gy were significantly longer compared to the 5-Gy treatment arm and untreated controls ($P < .05$), there was no significant difference between tumors treated with a total of 10 or 15 Gy. As a result, 5 Gy × 1 was selected as an intermediate, yet significant dose level for all subsequent orthotopic experiments. Of note, none of the irradiated mice experienced treatment-related morbidity or mortality within 2 weeks of treatment irrespective of the dose.

Tumor Targeting Accuracy

Using 2D-BLI fused offline to CBCT for tumor localization and image guidance as described previously, a single fraction of 5 Gy × 1 was delivered to orthotopic tumors using an anterior-posterior beam. Accurate targeting of the tumor was confirmed through identification and 2D localization of p-ATM and γ-H2Ax foci, which correlated to radiation-induced DNA damage and sites of repair. Coronal abdominal sections were generated orthogonal to the central beam axis to confirm

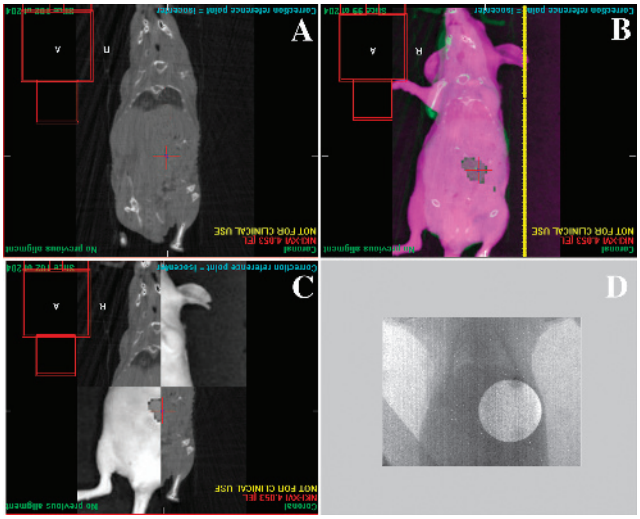

Figure 2. Radiation treatment planning and delivery to orthotopic pancreatic tumors. (A) Coronal CBCT image of anesthetized mouse obtained on the SARRP platform showing bony anatomy without clear ability to identify pancreatic tumor. (B) Offline bioluminescent coronal image of anesthetized mouse seen in A. Checkerboard fusion of images from A and B aligned to match external animal contour and identifiable internal anatomy showing excellent registration (C). (D) Double-exposure radiographs obtained in the treatment position on the SARRP identifying the radiation portal and confirming the area to be irradiated with 5 Gy in a single fraction (D).

irradiation of the entire tumor and general sparing of neighboring organs. This was more clearly identified through dissection and γ-H2Ax staining of individual organs (Figure 4*A*). The pancreatic tumor contained significantly more foci per cell (14.5) on average than the liver (0.31), greater (11.5) and lesser curvature (0.11) of the stomach, spleen (0.1), and unirradiated control (0.175; Figure 4*B*; $P < .05$). The

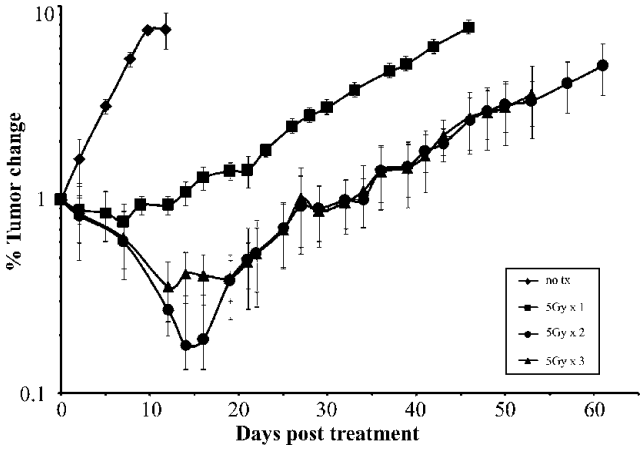

Figure 3. Radiation dose-response curve of heterotopic tumors. MiaPaCa-2–ELN flank tumors irradiated with 5, 10, or 15 Gy in 5-Gy daily fractions and assessed longitudinally show equal levels of significant inhibition with cumulative doses of 10 and 15 Gy and an intermediate level of growth inhibition with 5 Gy relative to untreated controls.

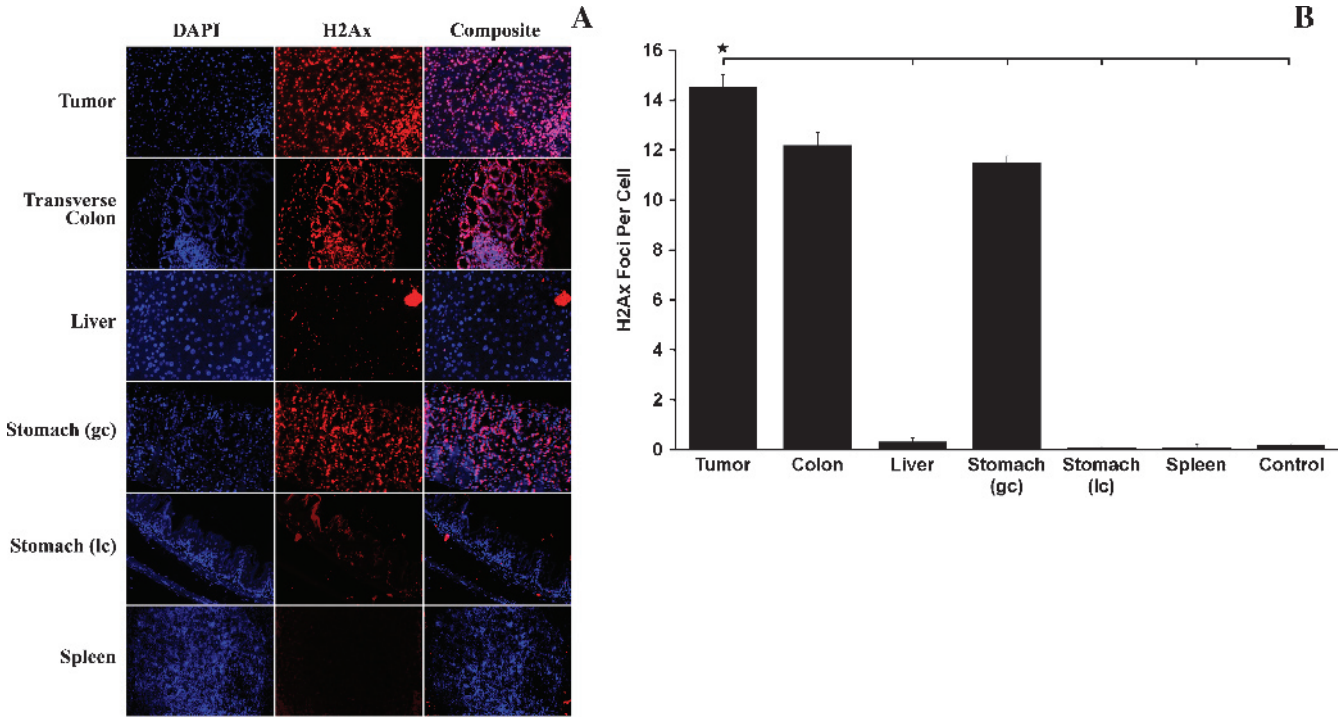

Figure 4. Staining with 4′,6-diamidino-2-phenylindole dihydrochloride and γ-H2Ax of abdominal organ dissected after focused abdominal radiation per Figure 3 shows intense colocalized staining of pancreatic tumor, as well as transverse colon and greater curvature of stomach, which were partly within the radiation field (A; original magnification, ×40). Other abdominal organs, including liver, lesser curvature of the stomach, and spleen, show minimal to no γ-H2Ax staining (A). Quantification of γ-H2Ax foci in A reported as the average sum of foci divided by the average number of nuclei in areas containing a minimum of 40 cells showing significantly higher quantities of staining in the pancreatic tumor relative to the liver, greater and lesser curvature of the stomach, spleen, and unirradiated control (B; $P < .05$).

transverse colon adjacent to the pancreatic tumor was calculated to have 12.2 γ-H2Ax foci per cell, which was not significantly different. Identification of the irradiated regions was further confirmed by p-ATM staining of individual organs, the patterns of which strongly correlated with those described above (data not shown).

Bioluminescence Monitoring of Radiation-Induced Orthotopic Tumor Growth Inhibition

After BLI-guided irradiation of orthotopic tumors (5 Gy × 1), mice were longitudinally monitored for TGI relative to untreated controls. At 30 days after treatment, irradiated tumors had a significantly lower mean photon emission of 7.1×10^9 p/s/cm^2/Sr compared to unirradiated tumors (2.1×10^{10} p/s/cm^2/Sr), representing a relative 2.97-fold inhibition of growth (Figure 5*F*). This was also confirmed pathologically at time of necropsy by measurement of the same tumors revealing a significant 3.5-fold decrease in the volume of treated relative to untreated tumors (Figure 5*C*; $P < .05$). Finally, using the same end point of a 10-fold increase in normalized tumor bioluminescence, mice were followed longitudinally, and a significant tumor growth delay of 24 days was observed with the irradiated (5 Gy × 1) mice relative to untreated controls ($n = 4$/group; $P < .05$; Figure 5*G*).

Discussion

The purpose of this study was to develop a biologically and clinically relevant radiation research model to facilitate preclinical testing of experimental therapeutics and sensitizers for the treatment of pancreatic cancer. Specifically, our goals were to apply the SARRP to a bioluminescent, orthotopic xenograft model to noninvasively: 1) allow identification of tumors and tumor burden before initiating therapy, thereby eliminating a potentially unidentifiable variable associated with randomization; 2) facilitate image-guided focal radiation therapy; and 3) normalization of tumor burden and longitudinal assessment of treatment response. We chose to use an orthotopic xenograft tumor model that closely mimicked the clinical presentation of pancreatic cancer patients and allowed tumors to grow in their native microenvironment. Indeed, limiting studies of potentially therapeutic agents to nonrepresentative preclinical models may provide an inaccurate profile of treatment efficacy and can have disappointing consequences when the agent is subsequently tested in the clinical setting [14]. Recent studies have shown that implantation of tumor cells ectopically *versus* orthotopically results in tumors with varying metastatic potential [15]. More specific to our study, Nakamura et al. [16] have shown a significant difference in gene expression patterns of cell line–derived orthotopic pancreatic tumors relative to the same tumors growing ectopically, thus highlighting the significant influence of the orthotopic microenvironment. A potential criticism of our study is the use of immortalized cell lines, albeit human and well characterized, which may or may not faithfully recapitulate human pancreatic cancer. Rubio-Viquera et al. [17] postulate that the *in vitro* adaptation of such lines may result in significant genetic alterations before orthotopic implantation, thus potentially altering the tumorigenic process. In our study, orthotopic tumors were found to eventually become not only locally invasive but also metastatic based on the anticipated hematogenous patterns of spread of disease. The inherent benefit of using immortalized lines is the ability to endogenously express luciferase,

which is not technically feasible with the use of primary human tumor explants. However, future studies are investigating the application of orthotopic xenografts established directly from patients with pancreatic cancer [17].

To our knowledge, a limited number of preclinical models evaluating irradiation of orthotopic tumor xenografts have been reported [18,19]. With the exception of the recent report by Lee et al. [9], none exist for pancreatic cancer. In addition, these studies used relatively imprecise methods of tumor targeting and radiation delivery, which certainly raises the possibility of not only missing the target, but also potentially overtreating nearby normal tissues, both of which could alter or confound the study's outcomes and limit the applicability of these data to contemporary radiation therapy used in the clinic. On the basis of these considerations, we focused on validating BLI as a noninvasive, facile means of providing image guidance for directing RT, and longitudinally monitoring tumors and subsequent response to therapy. Bioluminescence served as an accurate surrogate for pathologic tumor volume. In addition, when tumors were assessed longitudinally as a function of time, a linear increase in bioluminescent signal relative to tumor growth was noted until a plateau was reached. The plateau can likely be explained by the variable areas of hypoxia found within the larger tumors combined with the dependence of the luciferase reaction on oxygen [20]. On the basis of these data, we were confidently able to use BLI for longitudinal monitoring of tumors in the same animal over time, thereby eliminating the need for a substantial number of animals and facilitating accurate assessment of normalized tumor growth over time. Indeed, the costs, inefficiency, and potential lack of accuracy associated with invasive monitoring of treatment effect are an inherent criticism of many prospective preclinical studies.

Validation of BLI as a functional imaging surrogate was obtained through comparison with PET/CT. A major limitation of CBCT is its inability to adequately identify soft tissue tumors in the thorax and abdomen due to lack of contrast at lower imaging doses. Clinically, PET/CT is increasingly being used as the criterion standard for functional tumor imaging, thereby allowing accurate tumor staging and assessment of treatment response [21]. In addition, given the

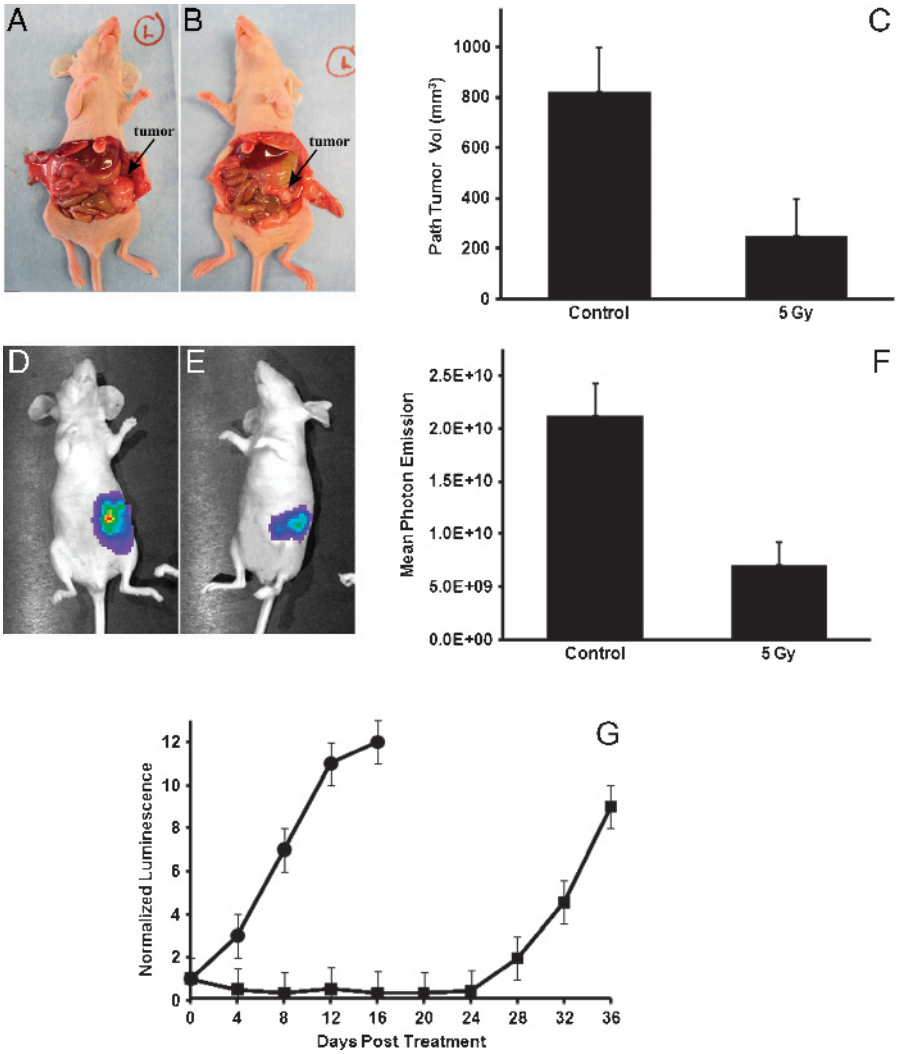

Figure 5. Longitudinal monitoring of bioluminescent orthotopic pancreatic tumors treated with or without 5 Gy of BLI-guided radiation shows treated tumors with a significantly lower tumor burden confirmed by pathologic (C) and mean photon emission mean (F) relative to respective controls. This is graphically depicted in the same animals in A and B and in D and E. When followed over time, irradiated tumors (■) showed a significant growth inhibition of 24 days compared to untreated tumors (●) using a 10× increase in tumor burden as an end point (G).

combination of functional and anatomic information provided in a single set of fused images, PET/CT is increasingly being used to more accurately guide radiation treatment planning in the clinic [22]. However, preclinical use of this modality is limited because of the time required per scan, the cost, as well as the potential for distress to the animals during prolonged sedation. Fusion of molecular optical imaging, such as BLI, with CT is done under the assumption that the functional image is an accurate spatial representation of the structural image. We validated this by correlating the BLI centroid with that of a focal, rigid radio-opaque surrogate of a tumor. The radial distances approximated each other quite well and dictated the need for a tumor margin expansion of approximately 4 mm to account for potential setup errors. Indeed, improved tumor localization obviates the need for larger irradiation fields and also helps minimize potentially confounding added toxicities, especially in abdominal malignancies such as pancreatic cancer. However, minimizing margins may also risk missing some of the tumor target. Similar to other functional imaging modalities, bioluminescence resulted in poor spatial resolution but provided an adjunctive means of identifying and targeting viable tumor when combined with CT images. Identification of double-stranded DNA damage and repair through p-ATM and γ-H2Ax staining confirmed our ability to accurately and repeatedly target the tumor while minimizing irradiation of normal tissues and associated toxicity. Given the lack of dosimetric treatment planning similar to that used in the clinic, γ-H2Ax quantitation was used as a potential surrogate biodosimeter. Previous studies have quantitated *in vivo* γ-H2Ax immunofluorescence and accurately correlated these levels to estimated radiation dose distributions [23]. Similarly in our study, normal organs at risk near the targeted tumor had comparable levels of γ-H2Ax foci. As a result, we assumed that the full dose was received by these regions comparable to the clinical setting when pancreatic tumors are irradiated and portions of the duodenum, small bowel, and liver receive close to the prescribed full dose.

Potential limitations of our study included the use of 2D optical imaging and offline methods for fusion to CT where the animal is transported between imaging modalities. At present, nonnegligible uncertainty exists with this method, which is potentially reduced with fusion of the optical image and on-board CBCT to guide animal placement. We have also used a single orthogonally directed beam as a simple model of irradiating the fused BLI-CBCT tumor target, which was sufficient for accurate targeting and more efficient for throughput treatment. Indeed, achieving a fully conformal 3D treatment volume using multiple radiation beams would be predicated on the successful fusion of a complementary 3D bioluminescent tomographic image and appropriate treatment planning. These studies are currently on going in our laboratory. Our initial radiation experiments attempted to identify the dose and fractionation scheme that led to an intermediate level of tumor growth delay without causing excessive treatment-related toxicities. During a course of 5 weeks, radiation-induced tumor growth inhibition was readily predicted by BLI and also confirmed pathologically. Bioluminescent disease progression was able to presage development of local symptoms (ascites, palpable tumor growth), thereby suggesting its use as a potential surrogate for estimating local tumor control and disease-free survival [24].

In summary, our studies confirm the ability to accurately and efficiently deliver RT to orthotopic pancreatic tumors in mice using a combination of molecular (BLI) and anatomic (CBCT) imaging while minimizing the dose to the surrounding normal tissues. BLI is a cost-effective surrogate for PET. It also allows for normalization of pretreatment tumor burden and quantitative, noninvasive monitoring of tumor progression in real time. This standardized preclinical RT platform provides the ability to closely mimic contemporary human RT and facilitate rapid, high-throughput evaluation of potential radiation sensitizers for pancreas cancer treatment.

References

[1] Jemal A, Siegel R, Ward E, Hao Y, Xu J, and Thun MJ (2009). Cancer statistics, 2009. *CA Cancer J Clin* **59**, 225–249.

[2] Herman JM, Swartz MJ, Hsu CC, Winter J, Pawlik TM, Sugar E, Robinson R, Laheru DA, Jaffee E, Hruban RH, et al. (2008). Analysis of fluorouracil-based adjuvant chemotherapy and radiation after pancreaticoduodenectomy for ductal adenocarcinoma of the pancreas: results of a large, prospectively collected database at the Johns Hopkins Hospital. *J Clin Oncol* **26**, 3503–3510.

[3] Neoptolemos JP, Stocken DD, Friess H, Bassi C, Dunn JA, Hickey H, Beger H, Fernandez-Cruz L, Dervenis C, Lacaine F, et al. (2004). A randomized trial of chemoradiotherapy and chemotherapy after resection of pancreatic cancer. *N Engl J Med* **350**, 1200–1210.

[4] Strimpakos A, Saif MW, and Syrigos KN (2008). Pancreatic cancer: from molecular pathogenesis to targeted therapy. *Cancer Metastasis Rev* **27**, 495–522.

[5] Stojadinovic S, Low DA, Hope AJ, Vicic M, Deasy JO, Cui J, Khullar D, Parikh PJ, Malinowski KT, Izaguirre EW, et al. (2007). MicroRT-small animal conformal irradiator. *Med Phys* **34**, 4706–4716.

[6] Zhou H, Rodriguez M, van den Haak F, Nelson G, Jogani R, Xu J, Zhu X, Xian Y, Tran PT, Felsher DW, et al. (2010). Development of a micro–computed tomography–based image-guided conformal radiotherapy system for small animals. *Int J Radiat Oncol Biol Phys* **78**, 297–305.

[7] Wong J, Armour E, Kazanzides P, Iordachita I, Tryggestad E, Deng H, Matinfar M, Kennedy C, Liu Z, Chan T, et al. (2008). High-resolution, small animal radiation research platform with x-ray tomographic guidance capabilities. *Int J Radiat Oncol Biol Phys* **71**, 1591–1599.

[8] Klerk CP, Overmeer RM, Niers TM, Versteeg HH, Richel DJ, Buckle T, Van Noorden CJ, and van Tellingen O (2007). Validity of bioluminescence measurements for noninvasive *in vivo* imaging of tumor load in small animals. *Biotechniques* **43**, 7–13, 30.

[9] Lee CJ, Spalding AC, Ben-Josef E, Wang L, and Simeone DM (2010). *In vivo* bioluminescent imaging of irradiated orthotopic pancreatic cancer xenografts in nonobese diabetic–severe combined immunodeficient mice: a novel method for targeting and assaying efficacy of ionizing radiation. *Transl Oncol* **3**, 153–159.

[10] Dalton WS (1999). The tumor microenvironment as a determinant of drug response and resistance. *Drug Resist Updat* **2**, 285–288.

[11] Bornmann C, Graeser R, Esser N, Ziroli V, Jantscheff P, Keck T, Unger C, Hopt UT, Adam U, Schaechtele C, et al. (2008). A new liposomal formulation of gemcitabine is active in an orthotopic mouse model of pancreatic cancer accessible to bioluminescence imaging. *Cancer Chemother Pharmacol* **61**, 395–405.

[12] Sun FX, Tohgo A, Bouvet M, Yagi S, Nassirpour R, Moossa AR, and Hoffman RM (2003). Efficacy of camptothecin analog DX-8951f (exatecan mesylate) on human pancreatic cancer in an orthotopic metastatic model. *Cancer Res* **63**, 80–85.

[13] Sawtell NM (2002). Preparation of single cells from solid tissues for analysis by PCR. *Curr Protoc Mol Biol* **Chapter 25**, Unit 25A 22.

[14] Voskoglou-Nomikos T, Pater JL, and Seymour L (2003). Clinical predictive value of the *in vitro* cell line, human xenograft, and mouse allograft preclinical cancer models. *Clin Cancer Res* **9**, 4227–4239.

[15] Fidler IJ (2003). The pathogenesis of cancer metastasis: the "seed and soil" hypothesis revisited. *Nat Rev Cancer* **3**, 453–458.

[16] Nakamura T, Fidler IJ, and Coombes KR (2007). Gene expression profile of metastatic human pancreatic cancer cells depends on the organ microenvironment. *Cancer Res* **67**, 139–148.

[17] Rubio-Viqueira B, Jimeno A, Cusatis G, Zhang X, Iacobuzio-Donahue C, Karikari C, Shi C, Danenberg K, Danenberg PV, Kuramochi H, et al. (2006). An *in vivo* platform for translational drug development in pancreatic cancer. *Clin Cancer Res* **12**, 4652–4661.

[18] Freytag SO, Paielli D, Wing M, Rogulski K, Brown S, Kolozsvary A, Seely J, Barton K, Dragovic A, and Kim JH (2002). Efficacy and toxicity of replication-competent adenovirus-mediated double suicide gene therapy in combination

with radiation therapy in an orthotopic mouse prostate cancer model. *Int J Radiat Oncol Biol Phys* **54**, 873–885.

[19] Sarkaria JN, Carlson BL, Schroeder MA, Grogan P, Brown PD, Giannini C, Ballman KV, Kitange GJ, Guha A, Pandita A, et al. (2006). Use of an orthotopic xenograft model for assessing the effect of epidermal growth factor receptor amplification on glioblastoma radiation response. *Clin Cancer Res* **12**, 2264–2271.

[20] Edinger M, Cao YA, Hornig YS, Jenkins DE, Verneris MR, Bachmann MH, Negrin RS, and Contag CH (2002). Advancing animal models of neoplasia through *in vivo* bioluminescence imaging. *Eur J Cancer* **38**, 2128–2136.

[21] Wahl RL, Jacene H, Kasamon Y, and Lodge MA (2009). From RECIST to PERCIST: evolving considerations for PET response criteria in solid tumors. *J Nucl Med* **50**(suppl 1), 122S–150S.

[22] Ford EC, Herman J, Yorke E, and Wahl RL (2009). ^{18}F-FDG PET/CT for image-guided and intensity-modulated radiotherapy. *J Nucl Med* **50**, 1655–1665.

[23] Horn S, Barnard S, and Rothkamm K (2011). γ-H2AX–based dose estimation for whole and partial body radiation exposure. *PLoS One* **6**, e25113.

[24] Hashizume R, Ozawa T, Dinca EB, Banerjee A, Prados MD, James CD, and Gupta N (2010). A human brainstem glioma xenograft model enabled for bioluminescence imaging. *J Neurooncol* **96**, 151–159.